Gradient index lens based combined two-photon microscopy and optical coherence tomography

Taejun Wang,[1,8,9] Qingyun Li,[2,8] Peng Xiao,[2] Jinhyo Ahn,[3] Young Eun Kim,[1] Youngrong Park,[4] Minjun Kim,[2] Miyeoun Song,[5] Euiheon Chung,[6] Wan Kyun Chung,[2] G-One Ahn,[1] Sungjee Kim,[4] Pilhan Kim,[3] Seung-Jae Myung,[7] and Ki Hean Kim[1,2,*]

[1]*Division of Integrative Biosciences and Biotechnology, Pohang University of Science and Technology, San 31, Hyoja-dong, Nam-gu, Pohang, Gyeongbuk 790-784, South Korea*
[2]*Department of Mechanical Engineering, Pohang University of Science and Technology, San 31, Hyoja-dong, Nam-gu, Pohang, Gyeongbuk 790-784, South Korea*
[3]*Graduate School of Nanoscience and Technology, Korea Advanced Institute of Science and Technology, Guseong-dong, Yusong-gu, Daejeon 305-701, South Korea*
[4]*Department of Chemistry, Pohang University of Science and TechnologySan 31, Hyoja-dong, Nam-gu, Pohang, Gyeongbuk 790-784, South Korea*
[5]*Research Center for Tooth and Periodontal Regeneration, Kyung Hee University School of Dentistry, 26 Kyungheedae-ro, Dongdaemun-gu, Seoul 130-872, South Korea*
[6]*Department of Medical System Engineering and School of Mechatronics, Gwangju Institute of Science and Technology, 123 Cheomdan-gwagiro, Buk-gu, Gwangju 500-712, South Korea*
[7]*Department of Gastroenterology, Asan Medical Center, University of Ulsan College of Medicine, 88 Olympic-ro, 43-gil, Songpa-gu, Seoul 138-736, South Korea*
[8]*These authors contributed equally to this work.*
[9]*tjwang@postech.ac.kr*
**kiheankim@postech.ac.kr*

Abstract: We report a miniaturized probe-based combined two-photon microscopy (TPM) and optical coherence tomography (OCT) system. This system is to study the colorectal cancer in mouse models by visualizing both cellular and structural information of the colon in 3D with TPM and OCT respectively. The probe consisted of gradient index (GRIN) lenses and a 90° reflecting prism at its distal end for side-viewing, and it was added onto an objective lens-based TPM and OCT system. The probe was 2.2 mm in diameter and 60 mm in length. TPM imaging was performed by raster scanning of the excitation focus at the imaging speed of 15.4 frames/s. OCT imaging was performed by combining the linear sample translation and probe rotation along its axis. This miniaturized probe based dual-modal system was characterized with tissue phantoms containing fluorescent microspheres, and applied to image mouse colonic tissues ex vivo as a demonstration. As OCT and TPM provided structural and cellular information of the tissues respectively, this probe based multi-modal imaging system can be helpful for in vivo studies of preclinical animal models such as mouse colonic tumorigenesis.

© 2014 Optical Society of America

OCIS codes: (170.2150) Endoscopic imaging; (170.2680) Gastrointestinal; (180.2520) Fluorescence microscopy; (180.4315) Nonlinear microscopy; (110.2760) Gradient-index lenses; (110.4500) Optical coherence tomography.

References and links

1. S. F. Pasha, J. A. Leighton, A. Das, M. E. Harrison, S. R. Gurudu, F. C. Ramirez, D. E. Fleischer, and V. K. Sharma, "Comparison of the yield and miss rate of narrow band imaging and white light endoscopy in patients undergoing screening or surveillance colonoscopy: a meta-analysis," Am. J. Gastroenterol. **107**(3), 363–371 (2012).
2. J. L. Matloff, W. Abidi, R. Richards-Kortum, J. Sauk, and S. Anandasabapathy, "High-resolution and optical molecular imaging for the early detection of colonic neoplasia," Gastrointest. Endosc. **73**(6), 1263–1273 (2011).

#208275 - $15.00 USD Received 14 Mar 2014; revised 24 Apr 2014; accepted 24 Apr 2014; published 21 May 2014

3. M. A. Kara, F. P. Peters, P. Fockens, F. J. ten Kate, and J. J. Bergman, "Endoscopic video-autofluorescence imaging followed by narrow band imaging for detecting early neoplasia in Barrett's esophagus," Gastrointest. Endosc. **64**(2), 176–185 (2006).
4. I. S. Ryu, S. H. Choi, H. Kim, M. W. Han, J. L. Roh, S. Y. Kim, and S. Y. Nam, "Detection of the primary lesion in patients with cervical metastases from unknown primary tumors with narrow band imaging endoscopy: preliminary report," Head Neck **35**(1), 10–14 (2013).
5. C. L. Zavaleta, E. Garai, J. T. C. Liu, S. Sensarn, M. J. Mandella, D. Van de Sompel, S. Friedland, J. Van Dam, C. H. Contag, and S. S. Gambhir, "A Raman-based endoscopic strategy for multiplexed molecular imaging," Proc. Natl. Acad. Sci. U.S.A. **110**(25), E2288–E2297 (2013).
6. S. J. Miller, C. M. Lee, B. P. Joshi, A. Gaustad, E. J. Seibel, and T. D. Wang, "Targeted detection of murine colonic dysplasia in vivo with flexible multispectral scanning fiber endoscopy," J. Biomed. Opt. **17**(2), 021103 (2012).
7. A. M. Winkler, P. F. Rice, J. Weichsel, J. M. Watson, M. V. Backer, J. M. Backer, and J. K. Barton, "In vivo, dual-modality OCT/LIF imaging using a novel VEGF receptor-targeted NIR fluorescent probe in the AOM-treated mouse model," Mol. Imaging Biol. **13**(6), 1173–1182 (2011).
8. N. Iftimia, A. K. Iyer, D. X. Hammer, N. Lue, M. Mujat, M. Pitman, R. D. Ferguson, and M. Amiji, "Fluorescence-guided optical coherence tomography imaging for colon cancer screening: a preliminary mouse study," Biomed. Opt. Express **3**(1), 178–191 (2012).
9. A. R. Tumlinson, L. P. Hariri, U. Utzinger, and J. K. Barton, "Miniature endoscope for simultaneous optical coherence tomography and laser-induced fluorescence measurement," Appl. Opt. **43**(1), 113–121 (2004).
10. J. Mavadia, J. Xi, Y. Chen, and X. Li, "An all-fiber-optic endoscopy platform for simultaneous OCT and fluorescence imaging," Biomed. Opt. Express **3**(11), 2851–2859 (2012).
11. S. Tang, Y. Zhou, K. K. Chan, and T. Lai, "Multiscale multimodal imaging with multiphoton microscopy and optical coherence tomography," Opt. Lett. **36**(24), 4800–4802 (2011).
12. L. P. Hariri, E. R. Liebmann, S. L. Marion, P. B. Hoyer, J. R. Davis, M. A. Brewer, and J. K. Barton, "Simultaneous optical coherence tomography and laser induced fluorescence imaging in rat model of ovarian carcinogenesis," Cancer Biol. Ther. **10**(5), 438–447 (2010).
13. Y. Pan, H. Xie, and G. K. Fedder, "Endoscopic optical coherence tomography based on a microelectromechanical mirror," Opt. Lett. **26**(24), 1966–1968 (2001).
14. I. N. Papadopoulos, S. Farahi, C. Moser, and D. Psaltis, "High-resolution, lensless endoscope based on digital scanning through a multimode optical fiber," Biomed. Opt. Express **4**(2), 260–270 (2013).
15. P. Kim, M. Puoris'haag, D. Côté, C. P. Lin, and S. H. Yun, "In vivo confocal and multiphoton microendoscopy," J. Biomed. Opt. **13**(1), 010501 (2008).
16. C. D. Saunter, S. Semprini, C. Buckley, J. Mullins, and J. M. Girkin, "Micro-endoscope for in vivo widefield high spatial resolution fluorescent imaging," Biomed. Opt. Express **3**(6), 1274–1278 (2012).
17. G. A. Sonn, S. N. Jones, T. V. Tarin, C. B. Du, K. E. Mach, K. C. Jensen, and J. C. Liao, "Optical biopsy of human bladder neoplasia with in vivo confocal laser endomicroscopy," J. Urol. **182**(4), 1299–1305 (2009).
18. C. M. Lee, C. J. Engelbrecht, T. D. Soper, F. Helmchen, and E. J. Seibel, "Scanning fiber endoscopy with highly flexible, 1 mm catheterscopes for wide-field, full-color imaging," J. Biophoton. **3**(5–6), 385–407 (2010).
19. C. Becker, M. C. Fantini, and M. F. Neurath, "High resolution colonoscopy in live mice," Nat. Protoc. **1**(6), 2900–2904 (2006).
20. C. Becker, M. C. Fantini, S. Wirtz, A. Nikolaev, R. Kiesslich, H. A. Lehr, P. R. Galle, and M. F. Neurath, "In vivo imaging of colitis and colon cancer development in mice using high resolution chromoendoscopy," Gut **54**(7), 950–954 (2005).
21. J. L. Dobbs, H. Ding, A. P. Benveniste, H. M. Kuerer, S. Krishnamurthy, W. Yang, and R. Richards-Kortum, "Feasibility of confocal fluorescence microscopy for real-time evaluation of neoplasia in fresh human breast tissue," J. Biomed. Opt. **18**(10), 106016 (2013).
22. T. Makino, M. Jain, D. C. Montrose, A. Aggarwal, J. Sterling, B. P. Bosworth, J. W. Milsom, B. D. Robinson, M. M. Shevchuk, K. Kawaguchi, N. Zhang, C. M. Brown, D. R. Rivera, W. O. Williams, C. Xu, A. J. Dannenberg, and S. Mukherjee, "Multiphoton tomographic imaging: a potential optical biopsy tool for detecting gastrointestinal inflammation and neoplasia," Cancer Prev. Res. **5**(11), 1280–1290 (2012).
23. L. E. Grosberg, A. J. Radosevich, S. Asfaha, T. C. Wang, and E. M. Hillman, "Spectral characterization and unmixing of intrinsic contrast in intact normal and diseased gastric tissues using hyperspectral two-photon microscopy," PLoS ONE **6**(5), e19925 (2011).
24. S. Zhuo, J. Yan, G. Chen, J. Chen, Y. Liu, J. Lu, X. Zhu, X. Jiang, and S. Xie, "Label-free monitoring of colonic cancer progression using multiphoton microscopy," Biomed. Opt. Express **2**(3), 615–619 (2011).
25. J. C. Jung, A. D. Mehta, E. Aksay, R. Stepnoski, and M. J. Schnitzer, "In vivo mammalian brain Imaging using one- and two-photon fluorescence microendoscopy," J. Neurophysiol. **92**(5), 3121–3133 (2004).
26. L. Fu, X. S. Gan, and M. Gu, "Characterization of gradient-index lens-fiber spacing toward applications in two-photon fluorescence endoscopy," Appl. Opt. **44**(34), 7270–7274 (2005).
27. H. C. Bao, J. Allen, R. Pattie, R. Vance, and M. Gu, "Fast handheld two-photon fluorescence microendoscope with a 475 μm × 475 μm field of view for in vivo imaging," Opt. Lett. **33**(12), 1333–1335 (2008).
28. C. Wang and N. Ji, "Pupil-segmentation-based adaptive optical correction of a high-numerical-aperture gradient refractive index lens for two-photon fluorescence endoscopy," Opt. Lett. **37**(11), 2001–2003 (2012).

#208275 - $15.00 USD Received 14 Mar 2014; revised 24 Apr 2014; accepted 24 Apr 2014; published 21 May 2014
(C) 2014 OSA

29. Y. Wu, Y. Leng, J. Xi, and X. Li, "Scanning all-fiber-optic endomicroscopy system for 3D nonlinear optical imaging of biological tissues," Opt. Express **17**(10), 7907–7915 (2009).
30. J. C. Jung and M. J. Schnitzer, "Multiphoton endoscopy," Opt. Lett. **28**(11), 902–904 (2003).
31. B. Jeong, B. Lee, M. S. Jang, H. Nam, S. J. Yoon, T. Wang, J. Doh, B. G. Yang, M. H. Jang, and K. H. Kim, "Combined two-photon microscopy and optical coherence tomography using individually optimized sources," Opt. Express **19**(14), 13089–13096 (2011).
32. J. K. Kim, W. M. Lee, P. Kim, M. Choi, K. Jung, S. Kim, and S. H. Yun, "Fabrication and operation of GRIN probes for in vivo fluorescence cellular imaging of internal organs in small animals," Nat. Protoc. **7**(8), 1456–1469 (2012).
33. P. Kim, E. Chung, H. Yamashita, K. E. Hung, A. Mizoguchi, R. Kucherlapati, D. Fukumura, R. K. Jain, and S. H. Yun, "In vivo wide-area cellular imaging by side-view endomicroscopy," Nat. Methods **7**(4), 303–305 (2010).
34. R. Suzuki, H. Kohno, S. Sugie, and T. Tanaka, "Dose-dependent promoting effect of dextran sodium sulfate on mouse colon carcinogenesis initiated with azoxymethane," Histol. Histopathol. **20**(2), 483–492 (2005).
35. J. G. Fujimoto, "Optical coherence tomography for ultrahigh resolution in vivo imaging," Nat. Biotechnol. **21**(11), 1361–1367 (2003).
36. S. Kozuka, "Premalignancy of the mucosal polyp in the large intestine: I. Histologic gradation of the polyp on the basis of epithelial pseudostratification and glandular branching," Dis. Colon Rectum **18**(6), 483–493 (1975).

1. Introduction

Colorectal cancer generally develops from abnormal growths of the large intestine such as adenomatous polyps, and its screening is usually performed by colonoscopic examination. A systemic review of tandem colonoscopy studies reported a pooled adenoma miss rate of 22% [1]. It is partly because the colon has folded structures and lesions can be hidden, and because there are flat lesions that are hard to detect by colonoscopy. There have been significant efforts in technological development in order to improve the diagnosis in various aspects [2]. Narrow-band and auto-fluorescence endoscopes, which visualize lesions in better contrasts than the conventional white-light endoscope by highlighting differences in vasculature and auto-fluorescence levels, have been developed and used in the clinic [3–5]. Various molecular markers targeting the colorectal cancer have been developed and tested in preclinical animal models in conjunction with fluorescent endoscopes [6–8]. Scanning endoscopes for optical coherence tomography (OCT), which can visualize under-surface tissue structures based on light back reflection, have been developed to detect lesions based on structural changes. These OCT endoscopes have been tried either alone or in combination with fluorescence detection as dual modalities [7–13].

In vivo distinction between the benign polyp and malignant colorectal cancer may be important to reduce the cost of pathologic examination. High-resolution endoscopes such as confocal and wide-field fluorescence micro-endoscopes have been developed [6, 14–18]. These high-resolution endoscopes can visualize cellular morphologies in conjunction with fluorescent probes, and may provide information of disease stages in situ without biopsy [2, 19–21]. These high-resolution modalities have been getting popular with commercial systems available. Two-photon microscopy (TPM), which is another high-resolution imaging modality, has been used to visualize cellular structures of colonic tissues without labeling based on auto-fluorescence [22–24], and various endoscopic probes for TPM have been developed [25–30]. Preclincal studies with animal models are important to test newly developed endoscopic imaging technologies or molecular probes targeting the colorectal cancer [19].

In this study, we developed a miniaturized probe based combined TPM and OCT system, which could be used for endoscopic dual-mode imaging of the mouse colon. The miniaturized probe, consisting of gradient index (GRIN) lenses and small optical elements, was integrated to a combined TPM and OCT system. Functions of OCT and TPM of the system were to screen lesions over large sections based on structural changes, and to closely examine lesions based on cellular molecular changes respectively. This dual-mode system was characterized with tissue-phantoms, and was applied to image mouse colonic tissues ex vivo as a demonstration.

#208275 - $15.00 USD Received 14 Mar 2014; revised 24 Apr 2014; accepted 24 Apr 2014; published 21 May 2014
(C) 2014 OSA

2. Materials and methods

2.1 System configuration

The system setup is shown in Fig. 1. The miniaturized imaging probe was added onto an objective lens based combined TPM and OCT system [31]. The combined system used two separate light sources for optimal imaging conditions of both modalities: a Ti-Sapphire laser (Chameleon Ultra II, Coherent) which has 140 fs pulse width and 80 MHz pulse repetition rate for TPM, and a wavelength-swept source (SSOCT-1310, Axsun) which has its center wavelength of 1310 nm, bandwidth of 103 nm, output power of 20 mW, and sweeping speed of 50 kHz for OCT. In TPM, an excitation beam from the source first passed through the power control unit composed of a half wave plate (HWP, 10RP52-4, Newport) and a polarizer (PL, GL5-B, Thorlabs). Then the beam was reflected on the x-y scanner (scan mirror, SM) consisting of a resonant scanner (8 kHz, Cambridge Technology) and a galvanometric scanner (6215H, Cambridge Technology), expanded by a pair of scan lens (SL) and tube lens (TL) by 2 times, transmitted through a dichroic mirror (DM2, 680DCLP, Chroma), and then coupled to an objective lens (OL, EC Plan-Neofluar, 20X, NA 0.5, Zeiss). The focus of excitation light by the objective lens was relayed to the sample by the miniaturized probe.

The miniaturized probe was a custom designed GRIN lens combination from GRINTECH, and it consisted of high numerical aperture (NA) coupling lenses (CL, NA 0.5, IFRL-200-023-50-NC) on both sides, a relay lens with low NA (RL, NA 0.1, IFRL-200-100-11-NC) in between, and a prism (PR, 1.3 mm in length) at its distal end to reflect light for side-viewing as shown in Fig. 2. The prism was attached at off-centered position of the GRIN lens in order to move the prism surface close to the outer surface of probe. The probe was protected by a stainless-steel tube, and its size was 2.2 mm in outer diameter and 60 mm in length. Focal plane of excitation light was formed approximately on the outer surface of probe including the metal tube, which was 350 μm away from the prism surface, so that the probe could do imaging by touching the sample. The focal plane could move up to 250 μm away from the probe surface by changing the distance between the objective and proximal end of the probe. The probe was inserted onto a holder consisting of two supporting bearings mounted on an x-y translator, which was to adjust the probe position with respect to the objective lens. Viewing orientation of the probe was adjusted by using a handle which was connected to the probe with a timing belt and pulleys. This holder design was adapted from the confocal endomicroscope [32].

Emission photons from the sample were collected by the probe and the objective lens followed by reflection DM2 entering into a photomultiplier tube (PMT, R5929, Hamamatsu). Real-time images were displayed on the computer screen. 3D images could be acquired by manually changing the distance between the objective lens and probe. An additional CCD camera was installed for bright-field imaging.

Regarding to OCT part, light from the source was delivered via an optical fiber and split to the sample and reference arms of an interferometry setup by 90/10 ratio. In the sample arm, light from the fiber was collimated to be 1 mm in diameter. This collimated beam was reflected by a flip mirror (FM), which was used to switch between OCT and TPM. The focused light by the objective lens was relayed to the sample by the probe. Since back aperture of the objective lens was 10 mm in diameter, the effective NA of the OCT beam was approximately 0.05. The scanning was implemented by both rotating the probe with a motor (Maxon motor #283838, EC-max, motor controller #347717, EPOS2, Switzerland) connected to the handle and by translating the sample linearly along the probe with a motorized stage (ST-SAN4505-150S + 3SR-AK42-B2, Sciencetown, Korea). Reflected light from the tissue sample was coupled back to the imaging probe and delivered to the same path as the illumination light in the reverse direction to the optical fiber. The reflected light from both the sample and the reference arms were combined at the detection arm and the interference signal

#208275 - $15.00 USD Received 14 Mar 2014; revised 24 Apr 2014; accepted 24 Apr 2014; published 21 May 2014
(C) 2014 OSA

was collected and processed. Dispersion difference between the reference and sample arms was compensated numerically by using pre-calibration data with a mirror sample.

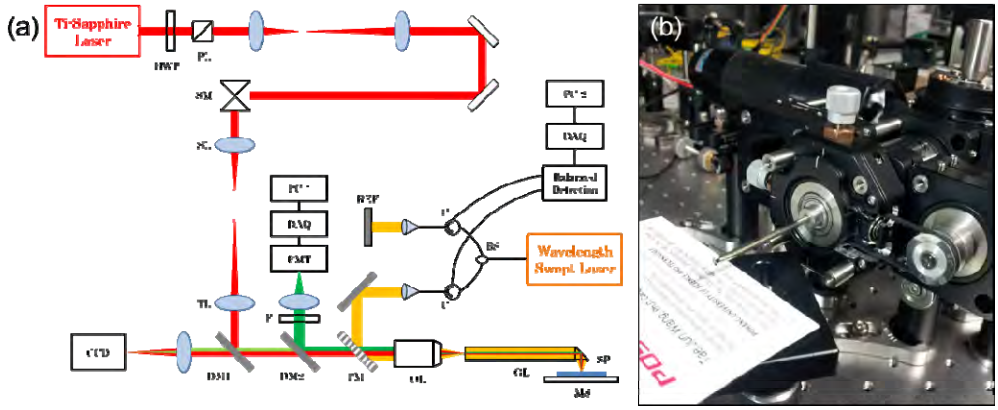

Fig. 1. A system schematic and a photograph of the imaging system. (a) System schematic. HWP: half-wave plate, PL: polarizer, SM: scanning mirror, SL: scanner lens, TL: tube lens, DM: dichroic mirror, F: filter, PMT: photomultiplier tube, FM: flip mirror, REF: reference arm, C: circulator, BS: beam splitter, OL: objective lens, GL: gradient index (GRIN) lens, SP: sample, MS: motorized stage. TPM excitation and emission beams, and OCT beams were depicted in red, green, and yellow colors respectively. (b) A photograph of the GRIN lens based imaging system.

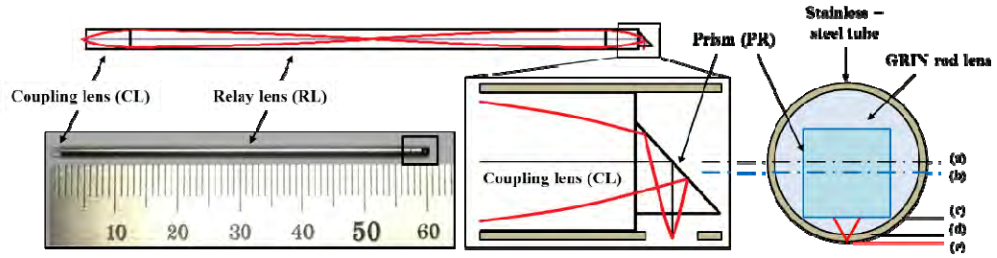

Fig. 2. A photograph and a schematic of the GRIN lens probe with ray tracing. (a) A centerline of the GRIN rod lens. (b) A centerline of the prism. (c) The prism surface. (d) The outer surface of GRIN rod lens. (e) The outer surface of stainless-steel tube.

2.2 System characterization

The system was characterized by imaging fluorescent microspheres, which were smaller than the resolutions of individual modalities. Microspheres of different sizes, 0.5 μm (F8813, yellow-green, 505/515, Invitrogen) and 6 μm (15716-5, 6 μm, yellow, Polysciences Inc.) in diameter, were used for TPM and OCT respectively. These microspheres were immobilized in agarose gel (2% in weight), and imaged in 3D. Images of individual microspheres were analyzed, and full widths at half maximum intensity (FWHMs) were measured by applying Gaussian curve fit to their intensity profiles. Results were summarized in Table 1. TPM resolutions were 1.06 μm and 8.13 μm in the lateral and axial directions respectively on average at the depth range from 0 μm to 50 μm. The resolutions were degraded with depth: 1.17 μm and 9.38 μm at the depth range from 100 μm to 150 μm, and 1.26 μm and 11.98 μm at the depth range from 200 μm to 250 μm. Standard deviations of all the measurement were within 20%. NA of the manufacturer's specification was 0.48, with which the ideal resolutions were 0.63 μm and 4.34 μm in the lateral and axial directions respectively. The manufacturer's NA specification turned out to indicate the maximum angle of light convergence only, not the quality of focus such as the resolution. Although the measured resolutions were less than the manufacturer's specification, they were comparable with the

#208275 - $15.00 USD Received 14 Mar 2014; revised 24 Apr 2014; accepted 24 Apr 2014; published 21 May 2014
(C) 2014 OSA

ones in the previous report [33]. Possible sources of the degradation may be the inherent aberration of GRIN lenses and some astigmatism. Field of view (FOV) of TPM was approximately 250 μm in diameter, and the imaging speed was 15.4 frames/s at maximum. OCT resolutions were 18 μm and 12 μm in the lateral and axial directions respectively in the air by under-filling the back aperture of objective lens, and they were close to theoretical calculations. OCT sensitivity was approximately 96.4 dB due to reflection from the objective lens and GRIN lens probe, which were anti-reflection (AR) coated for visible wavelength and uncoated respectively. The imaging speed was 40 mm/s at maximum for linear translation of the sample, and 1.6 rev/s for the probe rotation. The slow rotational speed was limited by the motor used in the current set up, and higher speeds can be achieved by using proper ones.

Table 1. Characteristic of the probe based system

	TPM	OCT
Lateral resolution	1.26 μm (at 125 μm depth)	18.0 μm
Axial resolution	11.98 μm (at 125 μm depth)	12.0 μm
Field of view (FOV)	250 μm x 250 μm	-
Imaging speed	15.4 frames/s	40.0 mm/s in translation, 1.6 rev/s in rotation

2.3 Sample preparation and imaging conditions

The new system was applied to image mouse colonic tissues of both the control and colorectal cancer models ex vivo. DsRed mice (B6-Tg(CAG-DsRed*MST) 1Nagy/J, 006051, Jackson Laboratory), which expressed DsRed fluorescent protein, were used in these experiments. These mice were bred at the animal facility of POSTECH Biotech Center under specific pathogen-free conditions. Both excised and intact colonic tissues were imaged. In case of the excised tissues, mice were euthanized and then colonic tissues were excised. The excised tissues were cut along the colon, flatten with the lumen side exposed, mounted on glass slides, and then fixed with 4% paraformaldehyde (PFA) solution. OCT imaging was performed by translating the tissue samples linearly with the stage, and regions of interest (ROIs) were searched from the OCT images. Once the ROIs were identified, the probe moved to those ROIs and TPM imaging was performed in 3D. In case of the intact colonic tissues, mice were euthanized right before the experiment. The probe was inserted into the colon through the anus up to a few tenth millimeters and the imaging was performed while the probe being pulled out. OCT imaging was performed by rotating the probe with the motor at several locations from the anus. TPM imaging was performed at the ROIs identified from the OCT imaging. The probe was positioned roughly at the center of the tubular colons for OCT imaging in order to avoid potential damage during its rotation. For the TPM imaging, the samples were shifted in the transverse direction of the probe in order for the probe to touch the lumen side of samples.

TPM excitation wavelength was tuned to 780 nm for DsRed protein excitation, and the excitation power was approximately 82 mW after the GRIN lens probe. Colonic tissues of a colorectal cancer model were imaged for comparison. In this model, the colorectal tumor was induced by applying azoxymethane (AOM) and dextran sulfate sodium (DSS) sequentially for 6 weeks [34]. Colonic tissues of the AOM-DSS model were prepared and imaged in the same way as the control ones.

3. Results

3.1 Normal colonic tissue, ex-vivo

OCT, TPM, and histological images of the normal mouse colon ex vivo are shown in Fig. 3. OCT imaging was performed by translating samples along the probe, and multiple images were acquired while shifting the samples in the transverse direction of the probe. OCT cross-

#208275 - $15.00 USD Received 14 Mar 2014; revised 24 Apr 2014; accepted 24 Apr 2014; published 21 May 2014
(C) 2014 OSA

sectional images in the x-z plane covering 25 mm in length show uniform layered micro-structures of the normal colon in Fig. 3(a). A zoomed image of a boxed region in Fig. 3(a) shows detail layered structures: mucosa (M), muscularis mucosa (MM) to submucosa (SM) boundary, muscularis externa (ME) from the lumen to serosa (S) in Fig. 3(b) [35]. A histological image in Fig. 3(c), which was haematoxylin and eosin (H&E) stained, shows good correlation with the OCT image. TPM images in the x-y plane at various depths are shown in Figs. 3(d)–3(g). These images were averaged by combining 15 frames from the real-time images to improve image contrast. The superficial epithelium and underlying cellular gland structures called “intestinal crypts” are shown. These crypts are circular in shape and uniformly distributed, which is typical for the normal colon. TPM movie clips with lateral and axial translation of the imaging plane were added in Media 1 and Media 2 respectively. These combined TPM and OCT images show both structural information at tenth micron scales and cellular information at sub-micron scales.

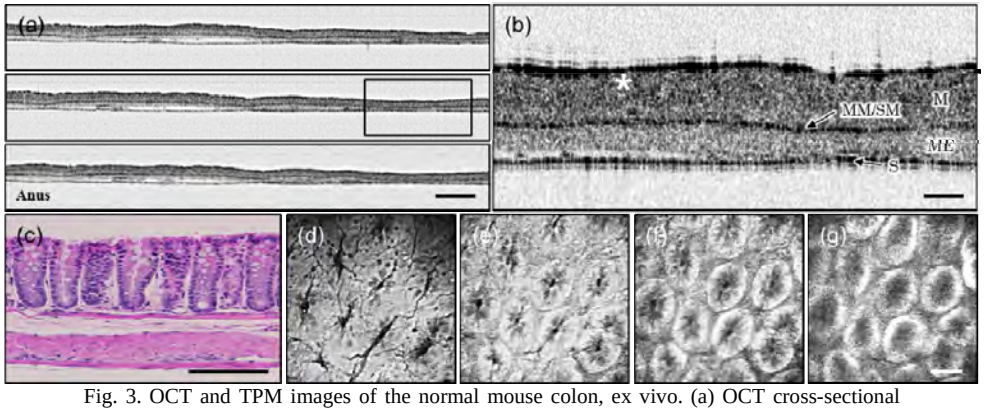

Fig. 3. OCT and TPM images of the normal mouse colon, ex vivo. (a) OCT cross-sectional images in the x-z plane along the colon covering 25 mm in length. Three images, which are parallel each other with 1.5 mm separation, are shown. The scale bar is 2 mm. (b) A zoomed OCT cross-sectional image of the normal region in a box of (a). An asterisk mark in (b) indicates the location of TPM imaging. The scale bar is 375 μm. (c) H&E stain histology of a normal colonic tissue. The scale bar is 100 μm. (d - g) TPM images in the x-y plane at various depths: epithelial layer at 10 μm deep from the surface, cellular gland structures at 15 μm, 50 μm, and 80 μm deep respectively. TPM movie clips with lateral and axial translation of the imaging plane were added in Media 1 and Media 2 respectively. The scale bar is 30 μm.

3.2 Colorectal cancer model, ex-vivo

OCT, TPM, and histological images of AOM-DSS colorectal cancer models ex vivo are shown in Fig. 4. Large sectional OCT images, a zoomed OCT image of the polyp are shown in Figs. 4(a) and 4(b) respectively. Large sectional OCT images show thickened mucosa on the left and a polyp in the center. The zoomed OCT image in Fig. 4(b) show thick superficial mucosa and some structures inside of the polyp. Different from the control case, boundary layers between the MM and SM are not clear in the polyp. The histological image in Fig. 4(c) shows similar features as the OCT image. These changes in the mucosa resulted from the tumorigenic process from hyperplastic to adenomatous [36]. TPM images of the polyp showed distorted gland structures as shown in Figs. 4(d) and 4(e). Individual cells are not resolvable in these images, partly due to the limitation of image resolution and DsRed protein distribution. Two TPM movie clips of the polyp regions were added in Media 3 and Media 4 respectively. Changes of layered structures and microscopic gland structures in the colorectal cancer model were clearly visualized.

3.3 Intact normal colonic tissue, ex-vivo

Endoscopic images of normal mouse colon ex vivo are shown in Fig. 5. OCT imaging was performed by rotating the probe, and reconstructed images at 3 different locations of 20 mm,

#208275 - $15.00 USD Received 14 Mar 2014; revised 24 Apr 2014; accepted 24 Apr 2014; published 21 May 2014
(C) 2014 OSA

15 mm, and 10 mm inside from the anus are shown in Figs. 5(a)–5(c) respectively. TPM images at different depths are shown in Figs. 5(d)–5(g). OCT images show layered structures of the normal colon from the lumen side. There are some regions where the layered structures are not clear, and this might be due to tissue folding or moisture issues inside the colon during imaging. A series of TPM images at different depth locations from the surface show typical glandular structures in this endoscopic imaging as well. A TPM movie clip with lateral and axial translation of the imaging plane was added in Media 5.

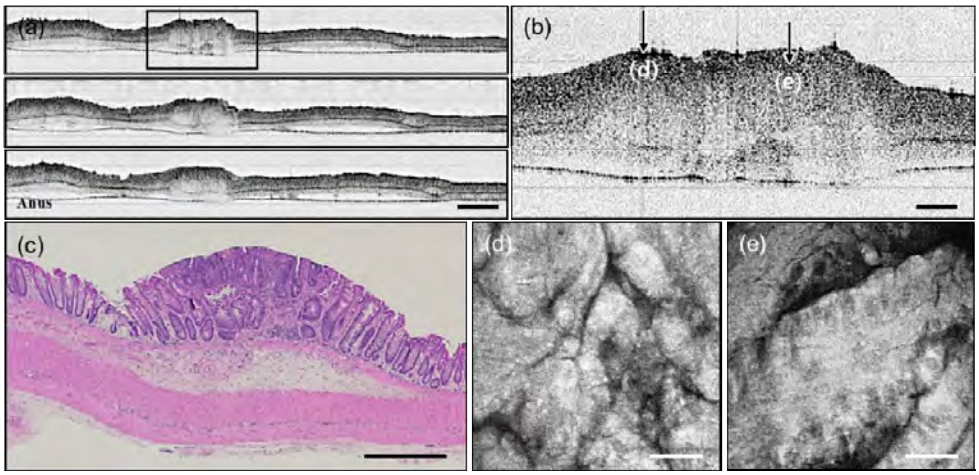

Fig. 4. OCT and TPM images of the AOM-DSS mouse colon, ex vivo. (a) OCT cross-sectional images in the x-z plane along the colon covering 25 mm in length. Three images, which are parallel each other with 1.5 mm separation, are shown. The scale bar is 2 mm. (b) A zoomed OCT cross-sectional image of the polyp in a box of (a). The scale bar is 375 μm. (c) H&E stain histology of the tumorous colonic tissue. The scale bar is 200 μm. (d, e) TPM images of the polyp in the x-y plane at different regions. Imaging depths were approximately 20 μm from the surface. TPM movie clips of the polyp regions were added in Media 3 and Media 4 respectively. The scale bar is 30 μm.

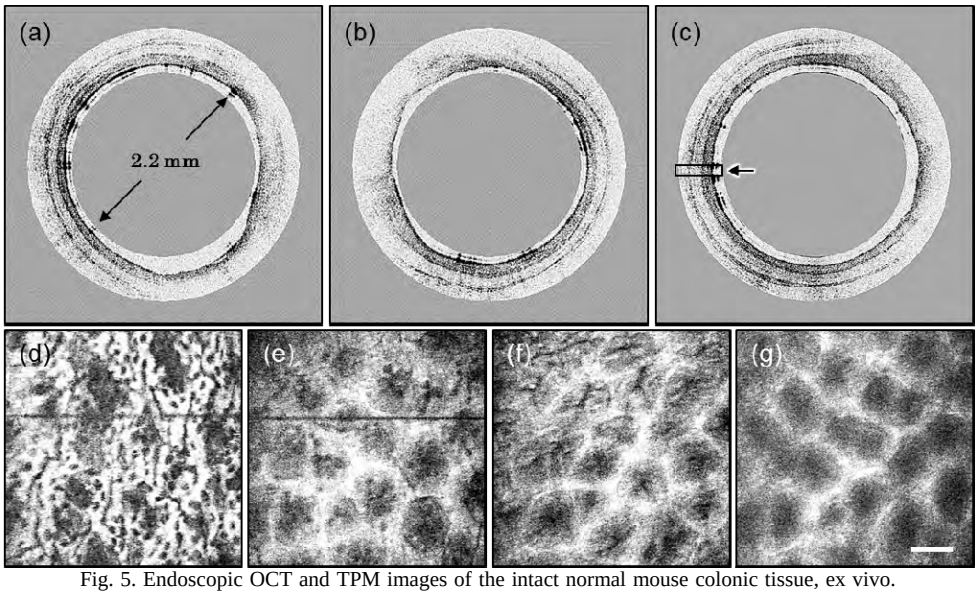

Fig. 5. Endoscopic OCT and TPM images of the intact normal mouse colonic tissue, ex vivo. (a - c) OCT cross-sectional images at various locations: 20 mm, 15 mm, and 10 mm inside from the anus respectively. (d - g) TPM images in the x-y plane at various depths: 10 μm, 20 μm, 40 μm, and 60 μm deep from the surface respectively. A TPM movie clip with lateral and axial translation of the imaging plane was added in Media 5. The scale bar is 30 μm.

#208275 - $15.00 USD Received 14 Mar 2014; revised 24 Apr 2014; accepted 24 Apr 2014; published 21 May 2014
(C) 2014 OSA

4. Discussions

A GRIN lens based combined TPM and OCT system was developed and tested by imaging tissue phantoms and ex-vivo colonic tissues of DsRed mice. Both structural and cellular information of the colon were obtained with the dual-mode imaging, and features of the normal and polyp cases were visualized by both modalities. The current dual-mode system used relatively high excitation power for TPM, partly due to some aberration of the GRIN lens probe and dispersion of excitation laser pulse. Excitation light was not well focused after the GRIN lens probe due to the astigmatism, which was found during the resolution measurement. This aberration might be due to relative large size of the current GRIN lens probe (2 mm in diameter) compared to the ones in previous reports (1 mm in diameter) [33]. We have been discussing with the manufacturer to resolve this issue. Further optimization is needed to improve the resolution and to reduce the input power. On-going works are to improve TPM image resolutions by either redesigning the probe or applying aberration compensation methods, and to do in vivo imaging. This novel system will enable in situ and in-vivo studies with preclinical small animal models.

Acknowledgments

This work is supported in part by the Bio and Medical Technology Development Program (No. 2011-0019633) and the Engineering Research Center grant (No. 2011-0030075) of the National Research Foundation (NRF) funded by the Korean government (MEST), and National R&D Program for Cancer Control (No. 1320220) by National Cancer Center Korea, and BK21 Plus (No. 10Z20130012243) funded by the Ministry of Education of Korea, and the Institute of Medical System Engineering in GIST, Korea.

#208275 - $15.00 USD Received 14 Mar 2014; revised 24 Apr 2014; accepted 24 Apr 2014; published 21 May 2014
(C) 2014 OSA